2015-03

Wave farm impact on beach modal state

Abanades, J

10.1016/j.margeo.2015.01.008
Marine Geology
Elsevier BV

Wave farm impact on beach modal state

J. Abanades[1*], D. Greaves[1], G. Iglesias[1]

[1] Plymouth University, School of Marine Science and Engineering, Marine Building, Drake Circus, Plymouth PL4 8AA, UK

ABSTRACT

The extraction of wave energy by the Wave Energy Converters (WECs) forming a wave farm results in a milder wave climate in its lee, which can have an impact on coastal processes. The objective of this work is to determine whether the beach morphology can be altered by the operation of the wave farm, and if so, to quantify this alteration. For this purpose, we examine how the farm affects the modal state of the beach with reference to a baseline (no farm) scenario. The modal state is defined based on an empirical classification that accounts for wave conditions, tidal regime and sediment size. As a beach typically goes through different modal states, we determine the percentages of time in an average year corresponding to each state in the baseline scenario, and how these percentages are altered by a wave farm as a function of its distance from the coast. This methodology is illustrated through a case study: Perranporth Beach (UK), an area of great potential for wave energy development. High-resolution numerical modelling is used, with two levels of grid refinement. We find that the wave farm has a relevant impact on the modal state of the system, which passes from wave-dominated to tide-dominated during significant periods of time. The sensitivity analysis, involving three cases with the farm at distances of 2 km, 4 km and 6 km from the beach, showed that the farm-to-coast distance plays a major role. Thus, the shift from a wave- to a tide-dominated beach is exacerbated in the case of the wave farm

*Corresponding author; e-mail: javier.abanadestercero@plymouth.ac.uk; tel.: +44.(0)7583 544041.

closest to the coastline, with the submarine bar vanishing over long periods of time. We conclude that the presence of the wave farm drastically alters the morphological response of the beach, and that this alteration is strongly dependent on the farm-to-coast distance.

Keywords: Wave energy; Wave farm; Nearshore impact; Beach morphology; conceptual beach model; Sediment transport

1. INTRODUCTION

Wave energy is poised to become one of the major renewable energies in a number of coastal regions around the world (Bernhoff et al., 2006; Carballo et al., 2014; Cornett, 2008; Defne et al., 2009; Gonçalves et al., 2014; Iglesias and Carballo, 2010a; Iglesias et al., 2009c; Lenee-Bluhm et al., 2011; Liberti et al., 2013; Stopa et al., 2011; Veigas et al., 2014a; Veigas and Iglesias, 2013; 2014; Vicinanza et al., 2013). The influence of wave energy extraction by the Wave Energy Converters (WECs) forming a wave farm on the nearshore wave conditions was recently shown by different authors (Carballo and Iglesias, 2013; Iglesias and Carballo, 2014; Mendoza et al., 2014; Millar et al., 2007; Palha et al., 2010; Ruol et al., 2011; Smith et al., 2012; Veigas et al., 2014b; Veigas et al., 2014c; Vidal et al., 2007; Zanuttigh and Angelelli, 2013). Abanades et al. (2014b) proved that this extraction resulted in a medium-term reduction of the erosion exceeding 20% in some sections of the beach profile (2D). In further studies, Abanades et al. (2014a); (2015) considered the 3D response of the beach under storm conditions in order to establish the applicability of wave farms to coastal defence. Erosion was found to decrease by more than 50% in certain areas of the beach. In the wake of these studies, which evidence the impact of wave farms on beach morphology, the question arises as to whether a wave farm can modify the modal state of a beach, and, if so, in what manner.

The objective of the present study is to answer this fundamental question by means of a case study: Perranporth Beach (UK). To quantify the effects of the wave farm on the modal state of the beach, scenarios with and without the farm were compared and the percentage of time corresponding to the different modal states during the period from 1st of November 2007 to 31st of October 2008 was determined. In addition, the

seasonal variability: “winter” (Nov-Apr) *vs* “summer” (May-Oct) was also examined. The modal states were established following the empirical classification presented by Masselink and Short (1993), based on Wright and Short (1984). The modal states vary as a function of the wave climate (breaking wave height and peak period), the beach sediment characteristics (sediment fall velocity) and the tidal regime (mean spring tidal range).

The effects of the wave farm on the coast are characterised using a wave propagation model, SWAN (Booij et al., 1996). The wave farm, which consists of eleven WaveCat WECs arranged in two rows, is implemented on a high-resolution grid so as to accurately resolve the wakes of the individual WECs, and hence that of the wave farm as a whole. Four scenarios are examined: three with the wave farm at different distances from a reference contour (10 m water depth): 2 km, 4 km and 6 km, following Abanades et al. (2015), plus the baseline scenario (without the wave farm). Thanks to the three distances considered it is possible to analyse the role of the farm-to-coast distance in the impact on the beach morphology. The WEC-wave field interaction is modelled by means of the wave transmission coefficient, obtained through laboratory tests as reported by Fernandez et al. (2012). The numerical model, successfully validated with wave buoy data, is used to calculate the wave conditions and on this ground establish the modal state of the beach.

The understanding and modelling of beaches is essential to coastal management (Budillon et al., 2006; Cowell et al., 1995; De Vriend et al., 1993; Hughes et al., 2014; Iglesias et al., 2009a; 2009b; Ortega-Sánchez et al., 2014; Ortega Sanchez et al., 2003; Poate et al., 2014). In the case of Perranporth, the beach was described as dissipative (Butt et al., 2001; Masselink et al., 2005) and as a low-tide bar rip system (Scott et al., 2011; Scott et al., 2007), with Austin et al. (2010) indicating that it is at the transition

between the low tide bar/rip and dissipative beach. In this context, the characterisation obtained in the present work contributes to understanding the behaviour of Perranporth by providing quantitative estimates of its morphodynamical variability throughout a year.

2. MATERIAL AND METHODS

1.1.1 CONCEPTUAL BEACH MODEL

The conceptual beach classifications are empirical models based on the relationships between the characteristics of different types of beaches (wave climate, sediment size and tidal regime) and field observations. Therefore, these models allow the evolution of beach dynamics as a function of the beach features to be predicted, and also, the quantification of the potential changes induced by a modification of these, such as the reduction of wave energy brought about by a wave farm.

The classification presented by Wright and Short (1984), also called the Australian beach model, is based on the field observations collected in Australia for microtidal beaches. This classification indicates the prevailing conditions in the surf zone: dissipative, intermediate or reflective, as a function of the dimensionless fall velocity parameter (Ω), also known as Dean's number (Dean, 1973),

$$\Omega = \frac{H_b}{w_s T} \tag{1}$$

where H_b is the breaking wave height, T is the wave peak period corresponding to the breaking conditions and w_s is the sediment fall velocity, which is defined for the present paper according the Shore Protection Manual (US Army Corps Of Engineers, 1984),

$$B = (\frac{\gamma_s}{\gamma_w} - 1)\frac{gD_{50}^3}{\nu^2} \tag{2}$$

$$w_s = \begin{cases} (\frac{\gamma_s}{\gamma_w} - 1)\frac{gD_{50}^2}{18\nu}; & B < 39, \\ (\frac{\gamma_s}{\gamma_w} - 1)^{0.7}\frac{g^{0.7}D_{50}^{1.1}}{6\nu^{0.4}}; & 39 < B < 10^4 \\ \left[(\frac{\gamma_s}{\gamma_w} - 1)\frac{gD_{50}}{0.91}\right]^{0.5}; & B > 10^4 \end{cases} \tag{3}$$

where γ_s and γ_w is the density of the sediment and water, respectively, g the gravitational acceleration, D_{50} the sediment grain size and ν the fluid kinematic viscosity.

This model represents the evolution of microtidal beaches well; however, it does not account for the influence of the tide on the swash, surf zone and shoaling wave processes (Davis and Hayes, 1984). This was corrected with the introduction of a new parameter: the Relative Tide Range (RTR), which allows the characterisation of all wave-dominated beaches in all tidal ranges (Masselink and Short, 1993):

$$RTR = \frac{MSR}{H_b}\ , \tag{4}$$

where *MSR* is the Mean Spring tidal Range.

Figure 1 shows the relationships between the dimensionless fall velocity and the relative tide range parameters that are used to establish the modal beach state. As the RTR parameter increases the beach evolves from a classic reflective state through the formation of a low tide terrace at the toe of the beach face and low tide rips to a steep beach face fronted by a dissipative low tide terrace. In the case of an intermediate barred

beach, the increase in the tidal range moves the bar down to the low tide level generating a low tide bar and rips. Finally, for barred dissipative beaches characterised by multiple subdued bars at different water depths, the increase of RTR results in the disappearance of these bars. The latter two groups shift to ultra-dissipative beaches with values of RTR between 7-15. For values of RTR greater than 15 the resulting beach is fully tide-dominated.

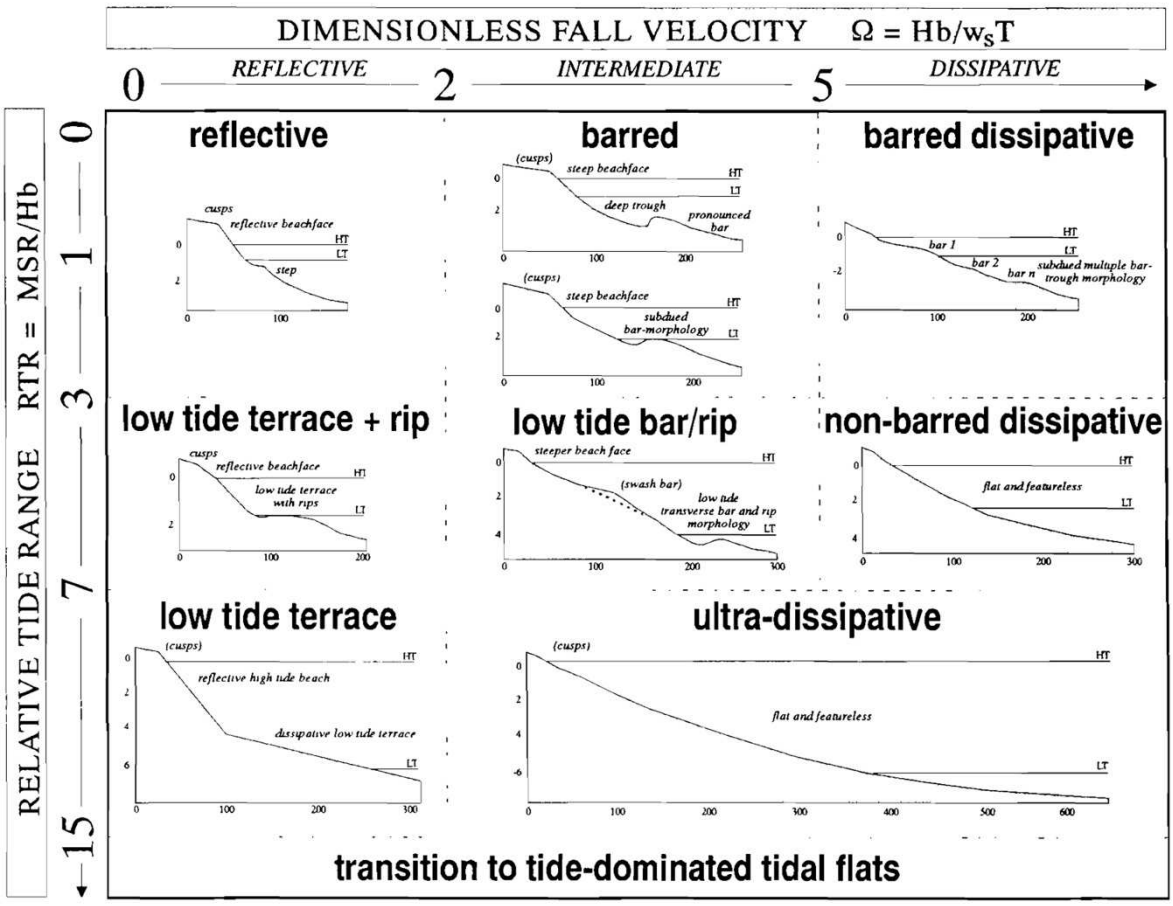

Figure 1: Conceptual beach model (Masselink and Short, 1993).

1.1.2 CASE STUDY: PERRANPORTH BEACH

The characterisation of the changes induced by a wave farm in the morphodynamical behaviour of a beach is conducted at Perranporth Beach (Figure 2), a prospective site for wave energy exploitation for its prime location on the Atlantic façade of Europe, which has been highlighted for its wave energy resource (Guedes

Soares et al., 2014; Iglesias and Carballo, 2009; 2010b; 2011; Pontes et al., 1996). An example of this potential is the Wave Hub project (Gonzalez-Santamaria et al., 2013; Reeve et al., 2011), a grid-connected offshore facility for sea tests of WECs, located in SW England. In addition to its wave energy potential, a further reason for choosing Perranporth is that this beach, facing directly the North Atlantic Ocean, has experienced increased erosion due to rising sea level and storminess – as corroborated by the extremely energetic storms of February 2014. Therefore, this would be a prime area for using a wave farm to control the storm-induced erosion (Abanades et al., 2014a; Abanades et al., 2014b; Abanades et al., 2015).

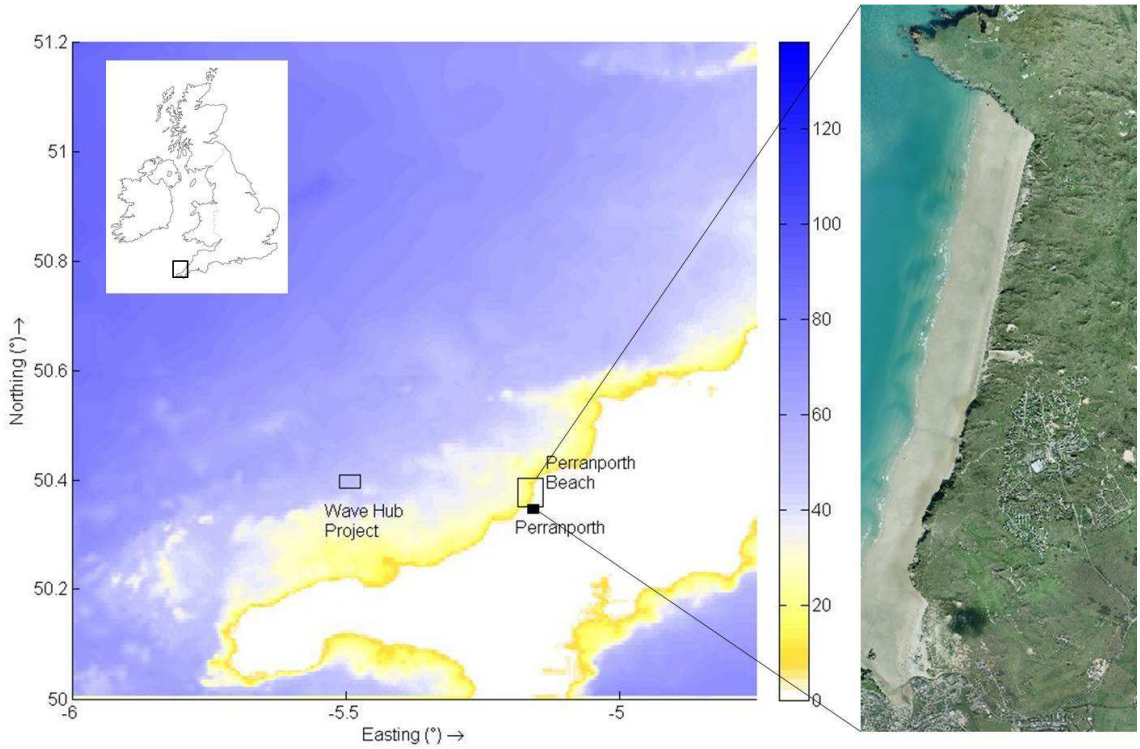

Figure 2: Bathymetry of SW England [water depths in m] including the location of Perranporth Beach, the WaveHub Project and an aerial photo of Perranporth Beach [source: Coastal Channel Observatory].

Perranporth is an approx. 4 km beach composed by a medium sand size, D_{50} = 0.27 – 0.29 mm, and characterised by a low intertidal slope, tan β = 0.015 – 0.025. In the present study, the offshore bathymetric data, from the UK data centre Digimap, and the

beach profile data, obtained through field survey by the Coastal Channel Observatory, are implemented onto the wave propagation model. In the three beach profiles selected to determine the beach modal state the relevant features can be readily observed (Figure 3): a submarine bar at a water depth between 5 and 10 m and a well-developed dune system that backs the landward end of the beach. The latter aspect does not play a role in the modal state, which only considers the intertidal area, but the bar system does – and is indicative of a dissipative or intermediate state. In the case of profile P3, two submarine bars are distinct – typical of a barred dissipative state.

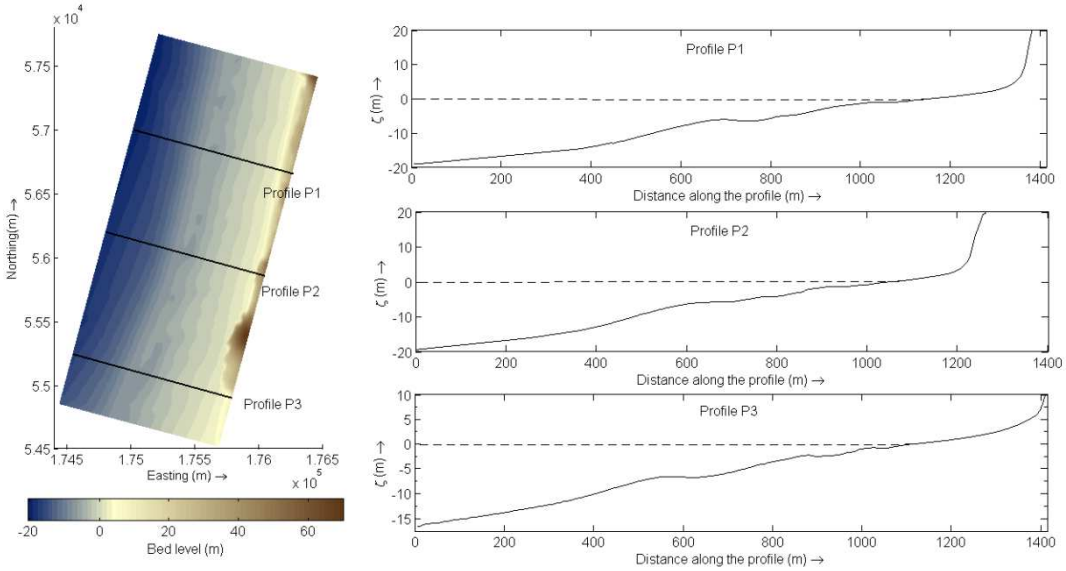

Figure 3: Three different profiles at Perranporth Beach and their respective localisation. Water depth in relation to local chart datum [in m].

As regards the wave conditions, wave buoy data are used in conjunction with hindcast data to force the wave propagation model. Hindcast data from WaveWatch III, a third-generation offshore wave model consisting of global and regional nested grids with a resolution of 100 km (Tolman, 2002), are used to prescribe the offshore boundary conditions. The validation is carried out with the wave buoy located off Perranporth Beach at a water depth of approx. 10 m. The average values of the significant wave height, peak period and direction from November 2007 to October

2008 were 1.60 m, 10.37 s and 282.59 °, respectively. Dividing this period into “winter” (Nov-Apr) and “summer” (May-Oct) to analyse the seasonal variability of the beach, the values in “winter” of the significant wave height, peak period and direction were 1.98 m, 11.30 s and 285.23 °, respectively, and in “summer” 1.32 m, 9.62 s and 279.95°.

Wind data from the Global Forecast System (GFS) weather model are also used as input of the wave model. In the period covered in the study the mean wind velocity magnitude at a height of 10 m above the sea surface (u_{10}) was 8.46 ms^{-1}. Strictly speaking there is no prevailing direction for the wind but the strongest winds, with velocities over 20 ms^{-1} come from the quarter between NE to NW.

Finally, the tide is also included in the model. At mentioned in the introduction, the large tidal range typical of SW England has a considerable effect on the beach morphodynamics. Perranporth is a macrotidal beach (*MSR* = 6.3 m) characterised by a semidiurnal regime.

1.1.3 WAVE PROPAGATION MODEL

The wave propagation is carried out using SWAN, a third-generation phase-averaged wave model for the simulation of waves in waters of deep, intermediate and shallow depth. SWAN computes the evolution of the wave spectrum based on the spectral wave action balance equation,

$$\frac{\partial \mathrm{N}}{\partial \mathrm{t}} + \nabla \cdot \left(\vec{\mathrm{c}}\mathrm{N}\right) + \frac{\partial \left(c_\theta \mathrm{N}\right)}{\partial \theta} + \frac{\partial \left(c_\sigma \mathrm{N}\right)}{\partial \sigma} = \frac{\mathrm{S}}{\sigma} \tag{5}$$

where N is the wave action density, t the time, $\vec{c}$ the propagation velocity in the geographical space, θ the wave direction, σ the relative frequency, and c_θ and c_σ the propagation velocity in the θ- and σ-space, respectively. The rate of change of wave action in time is given by the first term of equation (1), the second term represents the spatial propagation of wave

action and the third and fourth terms stand for the refraction and changes in the relative frequencies respectively induced by depth and currents. Finally, on the right-hand side, *S* is the source term and represents the generation and dissipation of energy density by the different processes involved.

A high-resolution grid is essential in this work in order to: (i) implement the WECs that formed the wave farm in their exact position, (ii) represent accurately the impact of the wave farm on the wave conditions in its lee, and (iii) determine the wave conditions to establish the morphodynamical state of the beach. On this basis, two computational grids are defined (Figure 4): (i) an offshore grid covering approx. 100 km × 50 km with a grid size of 400 × 200 m, and (ii) a high-resolution nearshore (nested) grid covering the study area, with dimensions of approx. 8 km × 6 km and a grid size of 16 m × 12 m.

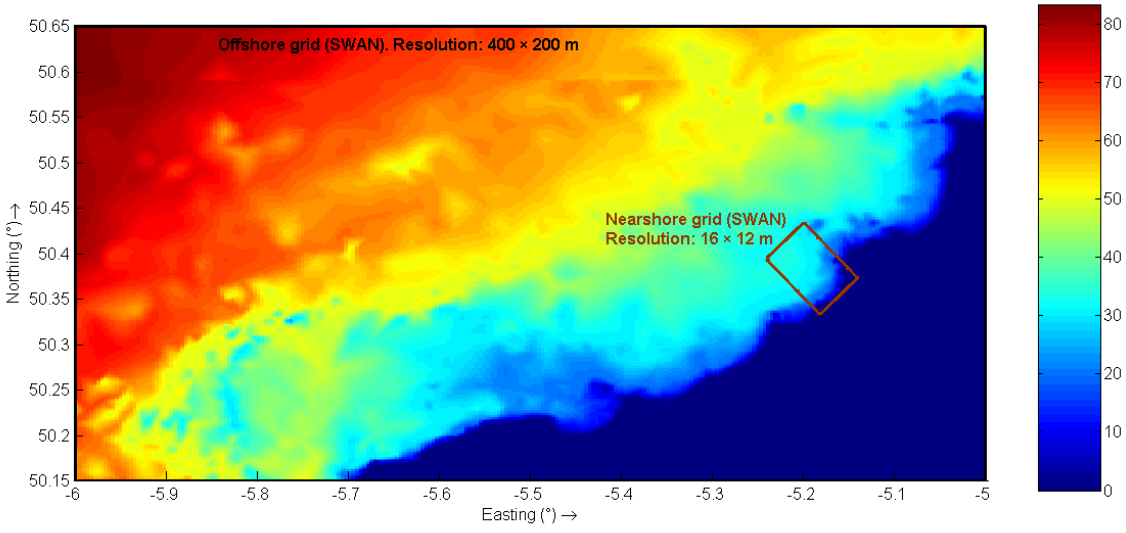

Figure 4: Computational grids of the wave propagation and the coastal processes model [water depths in m].

The wave farm consists of 11 WaveCat WECs arranged in two rows, with a spacing between devices equal to 2.2D, where D = 90 m is the distance between the twin bows of a single WaveCat WEC. The farm was located at distances of 2 km, 4 km, and 6 km (Figure 5) from a reference contour (10 m water depth), which corresponds to water depths of approx. 25 m, 30 m and 35 m, respectively (Carballo and Iglesias, 2013;

Iglesias and Carballo, 2014). The WEC-wave field interaction is modelled by means of the results obtained for the wave transmission coefficient in the lee of the device in the laboratory tests carried out by Fernandez et al. (2012). Compared with wave transmission, diffraction plays a minor role in analysing the effects of the WECs on the beach – the distance between the WECs and the reference 10 m contour (2000 m, 4000 m and 6000 m) being one order of magnitude larger than the width of the WECs (90 m). Therefore, the approximate solution of diffraction implemented on SWAN is sufficient for our purposes in this work.

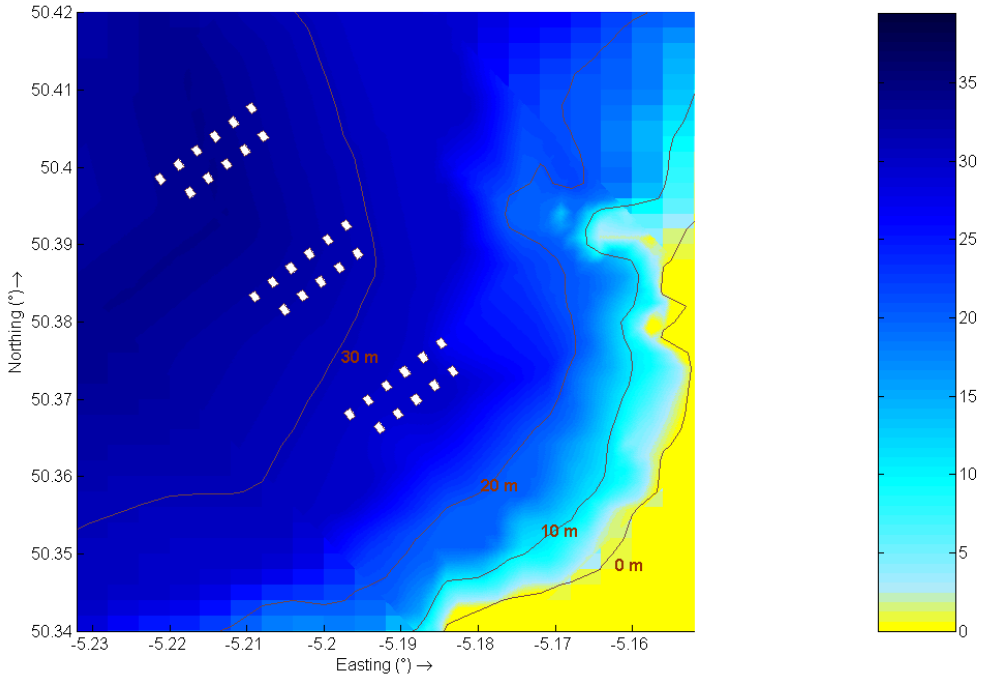

Figure 5: Wave farm located at different distances: 2 km, 4 km and 6 km to the 10 m water depth contour at Perranporth Beach [water depth in m].

The resource available is compared between the different scenarios through the average wave power of the wave farm, $\overline{J}$, in units of Wm^{-1} in the SI,

$$\overline{J} = \frac{\sum_{n=1}^{N} \sum_{t=1}^{T} (J_n)_t}{T} \quad , \tag{6}$$

where the index *n* represents a generic WEC of the wave farm, *N* is the total number of WECs (11), *t* a point in time, *T* the total number of time points studied (1 year) and $(J_n)_t$ the wave power at the *n*-WEC location at the *t* point of time, which is computed in SWAN as

$$J = \int_0^{2\pi} \int_0^{360} \rho g c E(\sigma,\theta)\, d\sigma\, d\theta \ , \tag{7}$$

where ρ is the water density, g is the acceleration due to gravity, and $E(\sigma,\theta)$ is the directional spectral density, which specifies how the energy is distributed over frequencies (σ) and directions (θ).

The effects caused by the farm in the different scenarios are assessed by means of the average Relative Nearshore Impact, $\overline{RNI}$ (Iglesias and Carballo, 2014), a non-dimensional impact indicator defined by

$$\overline{RNI}_i = \frac{1}{T}\frac{1}{S}\sum_{t=1}^{T}\sum_{s=1}^{S}\frac{J^{20}{}_b(s,t) - J^{20}{}_{f,i}(s,t)}{J^{20}{}_b(s,t)}, \tag{8}$$

where $J^{20}{}_{f,i}(s,t)$ is the wave power in the presence of the farm at a generic point (*s*) of the 20 m contour at a point of time (*t*), with the subindex *i* indicating the farm-to-coast distance (*i* = 2 km, 4 km or 6 km) and $J^{20}{}_b(s,t)$ is the baseline wave power (without the farm) at the same point, with *S* and *T* the total number of points along the contour and in time, respectively.

Finally, the wave conditions necessary to establish the morphological beach state – breaking wave height (H_b) and peak period (T_p) – are determined coupling the results from SWAN to the Kamphuis' formulae (Kamphuis, 1991), a breaking criterion for irregular waves based on the following expressions:

$$H_{sb} = 0.095 e^{4m} L_{bp} \tanh(\frac{2\Pi d_b}{L_{bp}}) \text{ , and} \quad (9)$$

$$\frac{H_{sb}}{d_b} = 0.56 e^{3.5m} \text{ ,} \quad (10)$$

where H_{sb} represents the breaking significant wave height, m the beach slope, L_{bp} the breaking wave length and d_b the breaking water depth. Once he breaking wave height was determined, the corresponding period was selected.

3. RESULTS AND DISCUSSION

First, the model is validated using the wave buoy data at Perranporth Beach from November 2007 to October 2008, missing out January 2008 owing to the lack of data. Figure 6 shows the good fit achieved between the significant wave height computed by SWAN and the values from the wave buoy. The coefficient of determination, R^2, and the Root Mean Square Error, *RMSE*, confirm the goodness of the fit: R^2 = 0.94 and *RMSE* = 0.38 m.

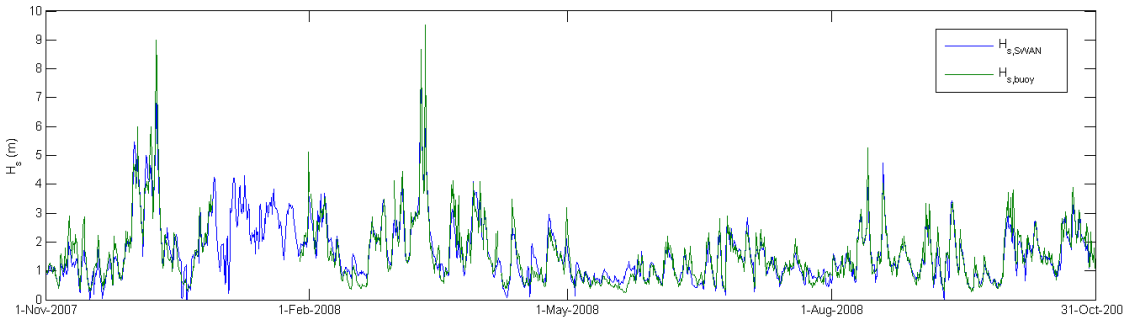

Figure 6: Time series of simulated ($H_{s,\,SWAN}$) and measured ($H_{s,\,buoy}$) significant wave height.

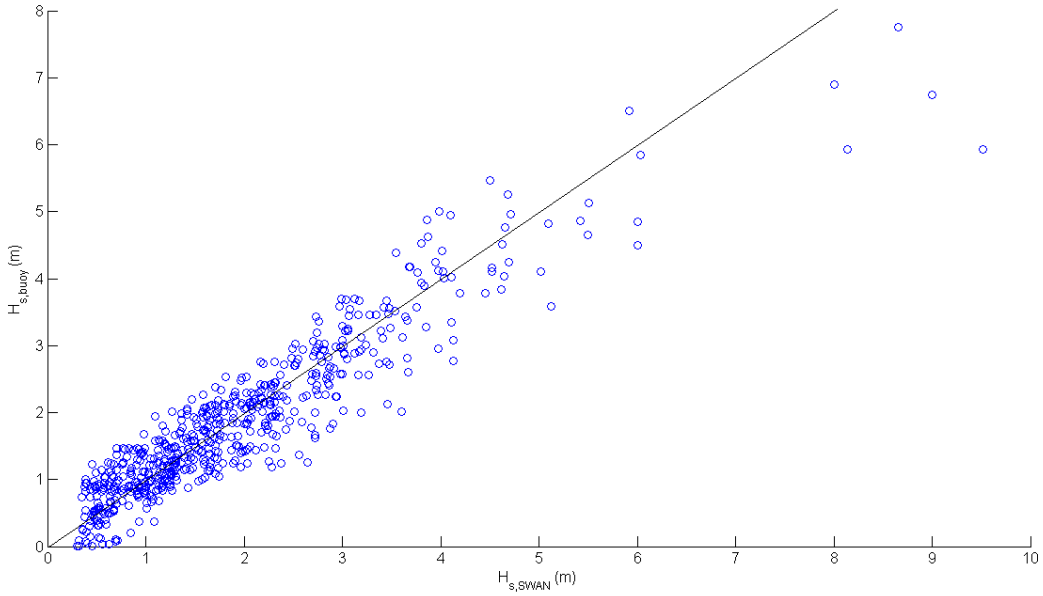

Figure 7: Scatter diagram: simulated ($H_{s,\,SWAN}$) vs. measured ($H_{s,\,buoy}$) significant wave height.

Second, the effects on the wave conditions of the wave farm scenarios are analysed and compared to the baseline scenario. Figure 8 shows the reduction of the significant wave height in the lee of the farm at a point in time. The greatest values of the reduction are found behind the second row of devices with values of approx. 40%, although these decrease towards the coast due to the wave energy diffracted from the sides into the wake of the farm. In the case of the wave farm at a distance of 2 km from the shoreline the reduction of the significant wave height at a water depth of 10 m at this point in time is 25%, while for the farm at 4 and 6 km the values is 12% and 5%, respectively.

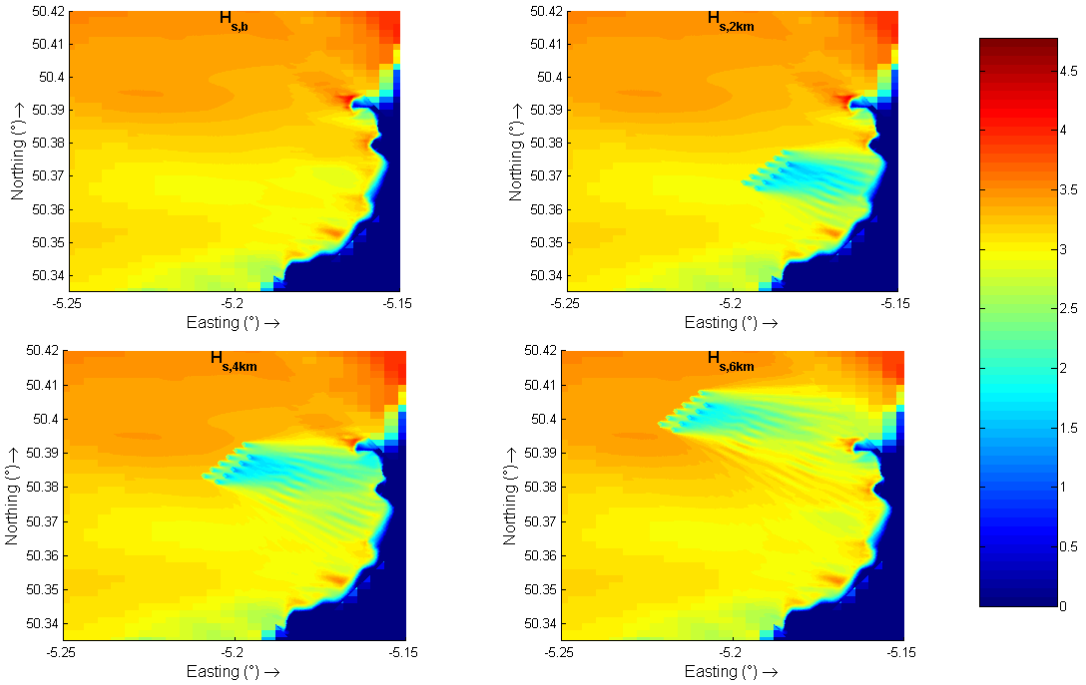

Figure 8: Significant wave height [m] in the baseline scenario ($H_{s,b}$) and in the presence of the farm at distances of 2 km ($H_{s,2km}$), 4 km ($H_{s,4km}$) and 6 km ($H_{s,6km}$) from the reference (10 m water depth) contour at 19th January 2014, 18:00 UTC [Deep water wave conditions: H_s = 4.69 m, T_p = 11.86 s and θ = 252.41°].

As regards the shadow caused by the wave farm, the area affected varies according to the wave direction, especially in the cases with a farm-to-coast distance of 4 and 6 km. The impact with waves coming from the east (Figure 8) is mainly focussed on the north area of the beach, whilst with waves from the NW the impact covers practically all the beach. In contrast, the impact of the wave farm closest to the beach does not vary with the wave conditions due to its proximity to the coast. Figure 9 illustrates the modification of the significant wave height in the different scenarios along the 20 m contour. It is observed that the greater the farm-to-coast distance, the larger the extension of the shadow; in the cases of the furthest and closest farm the shadow covers over 8 km and 3 km, respectively. However, the greatest impact of the furthest farm is outside of the beach limits for these offshore wave conditions.

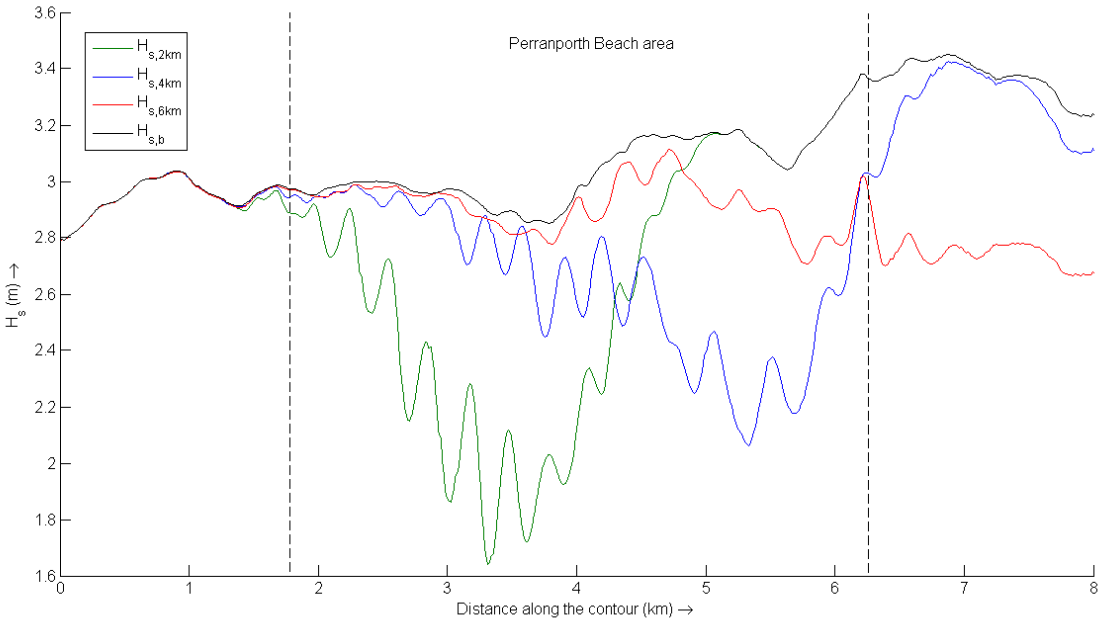

Figure 9: Significant wave height [m] in the baseline scenario ($H_{s,b}$) and in the presence of the farm at distances of 2 km ($H_{s,2km}$), 4 km ($H_{s,4km}$) and 6 km ($H_{s,6km}$) along the 20 m water depth contour at 19th January 2014, 18:00 UTC [Deep water wave conditions: H_s = 4.69 m, T_p = 11.86 s and θ = 252.41 °].

In terms of wave power reduction, the Relative Nearshore Impact indicator, $\overline{RNI}_i$, was defined to assess the average impact at a water depth contour of 20 m. The values for the different farm-to-coast distances are: $\overline{RNI}_{2km}$ = 25.59%, $\overline{RNI}_{4km}$ = 7.34% and $\overline{RNI}_{6km}$ = 2.66%. The reduction in wave energy is much more significant for the wave farm at 2 km, however, the overall resource for the wave farm at 2 km is 15% lower than that for the farm at 6 km (Table 1). The difference in terms of the available resource is less between the farm at 4 km and 6 km (5%). The results are also divided into "winter" (1st November - 31st April) and "summer" (1st May - 31st October) to assess the seasonal variability of wave power (approx. 70%), which, will be shown to affect the modal state of the beach.

Scenario	$\overline{J}$ (kW/m)		
	"Winter"	"Summer"	Average
2 km	239.98	78.15	159.01
4 km	275.72	86.07	180.83
6 km	288.28	91.49	189.82

Table 1: Average resource available in the wave farm for the different scenarios divided into "summer" (1st May - 31st October) and "winter" (1st November - 31st April)

Based on the results of the wave propagation model the modal state of the beach is determined. In order to investigate the spatial variability of the impact along with its seasonal variability, three profiles (Figure 3) are selected: profiles P1, P2 and P3 corresponded with the south, middle and north section of the beach.

First, the results for the south section of the beach are shown in Table 2. This section of the beach is predominantly dissipative (third column in the table), although the percentage that the beach is found to be intermediate (second column) is far from negligible. Indeed, in the case with the farm at a distance of 2 km, the low tide bar/rip becomes the most frequent state. The comparison between the baseline and farm scenarios reflects a slight modification of the modal state of the beach owing to the low impact of the wave farm on the wave conditions in this area. The maximum difference between the baseline and the farm scenarios is the case of the non-barred dissipative state, in which the reduction does not exceed 1%. In any case, the trends due to the reduction of the significant wave height are shown in the results; for instance, the percentage of low tide bar/rip state increases as the wave farm become closer, because the Relative Range Tidal parameter (*RTR*) is inversely proportional to the breaking wave height. On the other hand, the dimensionless fall velocity parameter (Ω) is directly proportional to the breaking wave height, and, therefore the barred dissipative state occurred more frequently in the baseline scenario than in the cases with the farm.

Profile P1: South section					
Reflective		Barred		Barred dissipative	
Baseline	0.00%	Baseline	0.07%	Baseline	16.04%
6 km	0.00%	6 km	0.07%	6 km	15.96%
4 km	0.00%	4 km	0.07%	4 km	15.90%
2 km	0.00%	2 km	0.07%	2 km	15.70%
Low tide Terrace + rip		Low tide bar/rip		Non-barred dissipative	
Baseline	0.00%	Baseline	25.50%	Baseline	26.59%
6 km	0.00%	6 km	25.70%	6 km	26.39%
4 km	0.00%	4 km	25.98%	4 km	26.18%
2 km	0.00%	2 km	26.18%	2 km	25.77%
Low tide terrace		Ultra-dissipative			
Baseline	3.36%	Baseline	22.89%		
6 km	3.36%	6 km	22.89%		
4 km	3.43%	4 km	22.82%		
2 km	3.36%	2 km	23.24%		
Transition to tide-dominated tidal flat					
Baseline		5.55%			
6 km		5.63%			
4 km		5.62%			
2 km		5.69%			

Table 2: Percentages of the beach modal state for the south section of the beach (Profile P1) from 1st November 2007 to 31st October 2008

Second, in the case of the middle of the beach (Table 3), the results were slightly different compared with the south section, due to the morphological differences between them (see Figure 3). In this area, the wave farm impacts are greater compared to the south section. Whereas the wave farm at 4 km and 6 km do not present significant differences compared with the baseline scenario, the wave farm at 2 km changes the behaviour of the beach significantly, reducing the barred dissipative state by more than 5% or 20 days per year, and increasing the ultradissipative state by more than 15 days. Overall, with the wave farm at 2 km the most frequent state shifted from non-barred dissipative (baseline) to ultra-dissipative due to the reduction of breaking wave height.

Profile P2: Middle section					
Reflective		Barred		Barred dissipative	
Baseline	0.00%	Baseline	0.07%	Baseline	21.73%
6 km	0.00%	6 km	0.07%	6 km	20.90%
4 km	0.00%	4 km	0.07%	4 km	20.29%
2 km	0.00%	2 km	0.00%	2 km	16.04%
Low tide Terrace + rip		Low tide bar/rip		Non-barred dissipative	
Baseline	0.00%	Baseline	22.76%	Baseline	26.11%
6 km	0.00%	6 km	22.69%	6 km	25.63%
4 km	0.00%	4 km	22.62%	4 km	25.29%
2 km	0.07%	2 km	23.85%	2 km	25.29%
Low tide terrace		Ultra-dissipative			
Baseline	2.06%	Baseline	22.69%		
6 km	2.19%	6 km	23.85%		
4 km	2.19%	4 km	24.81%		
2 km	3.29%	2 km	26.32%		
Transition to tide-dominated tidal flat					
Baseline		4.59%			
6 km		4.66%			
4 km		4.73%			
2 km		5.14%			

Table 3: Percentages of the beach modal state for the middle section of the beach (Profile P2) from 1st November 2007 to 31st October 2008

Third, the north section of the beach is the area that presented the greatest differences between the baseline and the farm scenarios (Table 4). The trends mentioned in previous paragraphs are accentuated in this area, the reduction in the barred and non-barred dissipative states results in a greater occurrence of the ultra-dissipative beach, from 5 days to 36 days per year in the case of the farm at 6 and 2 km, respectively – a very substantial change in the morphological behaviour of the beach. As regards the Ω parameter, it is observed that the closest wave farm make the low tide terrace and the low tide bar and rip states more frequent by 10 and 12 days per year, respectively, compared with the baseline scenario.

Profile P3: North section					
Reflective		Barred		Barred dissipative	
Baseline	0.00%	Baseline	0.14%	Baseline	16.59%
6 km	0.00%	6 km	0.07%	6 km	15.49%
4 km	0.00%	4 km	0.07%	4 km	14.39%
2 km	0.00%	2 km	0.07%	2 km	6.18%
Low tide Terrace + rip		Low tide bar/rip		Non-barred dissipative	
Baseline	0.00%	Baseline	28.10%	Baseline	28.71%
6 km	0.00%	6 km	27.55%	6 km	28.92%
4 km	0.00%	4 km	28.24%	4 km	28.71%
2 km	0.00%	2 km	31.11%	2 km	22.62%
Low tide terrace		Ultra-dissipative			
Baseline	0.89%	Baseline	22.68%		
6 km	0.96%	6 km	23.99%		
4 km	1.03%	4 km	24.40%		
2 km	3.49%	2 km	32.28%		
Transition to tide-dominated tidal flat					
Baseline		2.89%			
6 km		3.02%			
4 km		3.16%			
2 km		4.25%			

Table 4: Percentages of the beach modal state for the north section of the beach (Profile P3) from 1st November 2007 to 31st October 2008

Finally, regarding the seasonal variability, significant differences between "summer" and "winter" are found. These differences are analysed with reference to the north section (Table 5) for the sake of space – similar trends were found in the other sections. The main feature that distinguishes the winter from the summer is the presence of the bar in the baseline scenario. In winter, the beach is predominantly barred dissipative, what is usually called a "winter" or "storm" profile. The more energetic conditions increases the erosion, and lower the beach face as sand is moved offshore and deposited on submarine bars, which help to protect the beach by causing the waves to break further offshore. In summer, the state of the beach shifts from barred to non-barred – non-barred dissipative or ultra-dissipative – due to the milder wave conditions, and, therefore, the reduction of offshore sediment transport.

Profile P3: North section								
Reflective			**Barred**			**Barred dissipative**		
Scenario	Summer	Winter	Scenario	Summer	Winter	Scenario	Summer	Winter
Baseline	0.00%	0.00%	Baseline	0.00%	0.27%	Baseline	4.66%	28.53%
6 km	0.00%	0.00%	6 km	0.00%	0.14%	6 km	4.11%	26.89%
4 km	0.00%	0.00%	4 km	0.00%	0.14%	4 km	3.42%	25.38%
2 km	0.00%	0.00%	2 km	0.00%	0.14%	2 km	0.68%	11.66%
Low tide Terrace + rip			**Low tide bar/rip**			**Non-barred dissipative**		
Scenario	Summer	Winter	Scenario	Summer	Winter	Scenario	Summer	Winter
Baseline	0.00%	0.00%	Baseline	29.86%	26.34%	Baseline	29.59%	27.85%
6 km	0.00%	0.00%	6 km	29.59%	25.51%	6 km	29.18%	28.67%
4 km	0.00%	0.00%	4 km	30.00%	26.48%	4 km	28.63%	28.81%
2 km	0.00%	0.00%	2 km	27.67%	34.57%	2 km	18.77%	26.47%
Low tide terrace			**Ultra-dissipative**					
Scenario	Summer	Winter	Scenario	Summer	Winter			
Baseline	0.27%	1.51%	Baseline	33.15%	12.21%			
6 km	0.27%	1.65%	6 km	34.25%	13.72%			
4 km	0.41%	1.65%	4 km	34.79%	13.99%			
2 km	4.66%	2.33%	2 km	44.66%	19.89%			
Transition to tide-dominated tidal flat								
Scenario			Summer		Winter			
Baseline			3.29%		2.47%			
6 km			3.43%		2.60%			
4 km			3.57%		2.74%			
2 km			4.94%		3.56%			

Table 5: Percentages of the beach modal state for the north section of the beach (Profile P3) in "summer" (1st November 2007 - 31st April 2008) and "winter" (1st May 2008 - 31st October 2008)

In the scenarios with the farm this seasonal behaviour changes specially with the farm at 2 km. In winter, the barred dissipative state becomes less frequent in favour of ultra-dissipative and low tide bar/rip states. In the latter, the beach keeps the bar system but enlarges the intertidal flat, with the result that the system behaves as an intermediate beach at mid tide, reflective at high tide and dissipative at low tide. By contrast, in summer, the increase of the occurrence of ultra-dissipative state is very significant given that the beach behaves according this state during almost half of the summer.

In summary, Perranporth beach is found to be at the transition between the low tide bar/rip and dissipative beach states in the scenario without the farm. Despite the spatial variations between the different profiles, the greatest differences are observed in the seasonal study. The absence of the bar distinguished the behaviour of the beach during summer from winter. However, the presence of the wave farm affects the modal state of the beach drastically, decreasing the occurrence of wave-dominated states (barred and non-barred dissipative states) in the favour of tide-dominated (low tide bar and rip in winter and ultra-dissipative in summer). The reduction of the breaking wave height brought about by the wave farm (~18%, comparing the baseline scenario with the nearest farm) results in a significant modification of the morphological response of the beach. The reduction of the wave-dominated states would seem to lead to an increase in the onshore sediment transport and the removal of the offshore bar, the materials of which would cause accretion on the beach – in line with the findings by Abanades et al. (2014a); (2014b).

4. CONCLUSIONS

In view of the accelerated pace of development of wave energy, a thorough understanding of the effects of nearshore wave farms on beach morphodynamics will soon be fundamental to coastal management. This paper examines these effects with reference to the modal state of the beach using an empirical classification based on wave conditions, sediment size and tidal regime. The spatial and temporal changes to the modal state of the beach induced by the wave farm are investigated. To resolve accurately the wake of the individual WECs in the farm, a state-of-the-art wave propagation model is implemented on a high-resolution grid. To assess the influence of

the farm-to-coast distance, a sensitivity analysis is carried out with a wave farm located at different distances from the coast.

We find that the farm-to-coast distance plays a major role, and that the wave farm closest to the shoreline (2 km) substantially alters the nearshore wave conditions. For instance, the reduction of wave power along the 20 m contour exceeds 25% over a 3 km stretch of coastline. In contrast, the reduction in the case of the furthest wave farm is under 10%, extending over 8 km of coastline. This milder nearshore wave climate, brought about by the wave farm, is shown to modify the morphological behaviour of the beach. In the baseline scenario, Perranporth Beach is at the transition between the low tide bar/rip and dissipative states. The modal state varies along the beach, although large spatial differences are not observed concurrently. However, the seasonal variability is far more pronounced. In winter the beach is wave-dominated, the energetic wave conditions increasing offshore sediment transport and forming a submarine bar. In summer, under milder wave conditions, the beach is tide-dominated.

We also find that the wave farm modify the morphological behaviour of the beach significantly, especially in its north and middle section, where the wave height reduction is more apparent. The predominant character of the beach is transformed from wave- to tide-dominated. For instance, in the north section the predominant state is a low tide bar/rip in the baseline scenario, which turns into a ultra-dissipative system in the case of the nearest (2 km) wave farm. In this case the wave-dominated states are reduced by over 10%, or over 36 days per year. This modification also occurs in the cases with farm-to-coast distances of 4 km and 6 km, albeit to a lesser extent: the barred dissipative states become less frequent (by up to 10 days per year) and accordingly, the tide-dominated states, e.g., ultra-dissipative or transition to tide-dominated tidal flat, occur more often. The reduction in the occurrence of the barred states corresponds to an

increase of the onshore sediment transport and the removal of the offshore bar, which would in turn lead to accretion of the beach.

In sum, this work showed that a wave farm can alter the behaviour of a beach in its lee considerably. This in itself need not be regarded as a negative impact; on the contrary, the wave farm can lead to beach accretion and thus serve to counter erosional trends. Moreover, the effects of the wave farm on the beach can be controlled by locating the farm closer to, or further from, the shoreline.

5. REFERENCES

Abanades, J., Greaves, D. and Iglesias, G., 2014a. Coastal defence through wave farms. Coastal Engineering, 91(0): 299-307.

Abanades, J., Greaves, D. and Iglesias, G., 2014b. Wave farm impact on the beach profile: A case study. Coastal Engineering, 86(0): 36-44.

Abanades, J., Greaves, D. and Iglesias, G., 2015. Coastal defence using wave farms: The role of farm-to-coast distance. Renewable Energy, 75(0): 572-582.

Austin, M. et al., 2010. Temporal observations of rip current circulation on a macro-tidal beach. Continental Shelf Research, 30(9): 1149-1165.

Bernhoff, H., Sjöstedt, E. and Leijon, M., 2006. Wave energy resources in sheltered sea areas: A case study of the baltic sea. Renewable Energy, 31(13): 2164-2170.

Booij, N., Holthuijsen, L. and Ris, R., 1996. The" swan" wave model for shallow water. Coastal engineering conference, p.^pp. 668-676.

Budillon, F., Vicinanza, D., Ferrante, V. and Iorio, M., 2006. Sediment transport and deposition during extreme sea storm events at the salerno bay (tyrrhenian sea): Comparison of field data with numerical model results. Natural Hazards and Earth System Science, 6(5): 839-852.

Butt, T., Russell, P. and Turner, I., 2001. The influence of swash infiltration–exfiltration on beach face sediment transport: Onshore or offshore? Coastal Engineering, 42(1): 35-52.

Carballo, R. and Iglesias, G., 2013. Wave farm impact based on realistic wave-wec interaction. Energy, 51: 216-229.

Carballo, R., Sánchez, M., Ramos, V., Taveira-Pinto, F. and Iglesias, G., 2014. A high resolution geospatial database for wave energy exploitation. Energy, 68(0): 572-583.

Cornett, A.M., 2008. A global wave energy resource assessment. ISOPE--579

Cowell, P., Roy, P. and Jones, R., 1995. Simulation of large-scale coastal change using a morphological behaviour model. Marine Geology, 126(1): 45-61.

Davis, R.A. and Hayes, M.O., 1984. What is a wave-dominated coast? Marine Geology, 60(1): 313-329.

De Vriend, H. et al., 1993. Approaches to long-term modelling of coastal morphology: A review. Coastal Engineering, 21(1): 225-269.

Dean, R.G., 1973. Heuristic models of sand transport in the surf zone. First Australian Conference on Coastal Engineering, 1973: Engineering Dynamics of the Coastal Zone, p.^pp. 215.

Defne, Z., Haas, K.A. and Fritz, H.M., 2009. Wave power potential along the atlantic coast of the southeastern USA. Renewable Energy, 34(10): 2197-2205.
Fernandez, H. et al., 2012. The new wave energy converter wavecat: Concept and laboratory tests. Marine Structures, 29(1): 58-70.
Gonçalves, M., Martinho, P. and Guedes Soares, C., 2014. Assessment of wave energy in the canary islands. Renewable Energy, 68(0): 774-784.
Gonzalez-Santamaria, R., Zou, Q.-P. and Pan, S., 2013. Impacts of a wave farm on waves, currents and coastal morphology in south west england. Estuaries and Coasts: 1-14.
Guedes Soares, C., Bento, A.R., Gonçalves, M., Silva, D. and Martinho, P., 2014. Numerical evaluation of the wave energy resource along the atlantic european coast. Computers & Geosciences, 71(0): 37-49.
Hughes, M.G., Aagaard, T., Baldock, T.E. and Power, H.E., 2014. Spectral signatures for swash on reflective, intermediate and dissipative beaches. Marine Geology, 355(0): 88-97.
Iglesias, G. and Carballo, R., 2009. Wave energy potential along the death coast (spain). Energy, 34(11): 1963-1975.
Iglesias, G. and Carballo, R., 2010a. Offshore and inshore wave energy assessment: Asturias (n spain). Energy, 35(5): 1964-1972.
Iglesias, G. and Carballo, R., 2010b. Wave energy and nearshore hot spots: The case of the se bay of biscay. Renewable Energy, 35(11): 2490-2500.
Iglesias, G. and Carballo, R., 2011. Choosing the site for the first wave farm in a region: A case study in the galician southwest (spain). Energy, 36(9): 5525-5531.
Iglesias, G. and Carballo, R., 2014. Wave farm impact: The role of farm-to-coast distance. Renewable Energy, 69(0): 375-385.
Iglesias, G., López, I., Carballo, R. and Castro, A., 2009a. Headland-bay beach planform and tidal range: A neural network model. Geomorphology, 112(1–2): 135-143.
Iglesias, G., López, I., Castro, A. and Carballo, R., 2009b. Neural network modelling of planform geometry of headland-bay beaches. Geomorphology, 103(4): 577-587.
Iglesias, G. et al., 2009c. Wave energy potential in galicia (nw spain). Renewable Energy, 34(11): 2323-2333.
Kamphuis, J., 1991. Wave transformation. Coastal Engineering, 15(3): 173-184.
Lenee-Bluhm, P., Paasch, R. and Özkan-Haller, H.T., 2011. Characterizing the wave energy resource of the us pacific northwest. Renewable Energy, 36(8): 2106-2119.
Liberti, L., Carillo, A. and Sannino, G., 2013. Wave energy resource assessment in the mediterranean, the italian perspective. Renewable Energy, 50: 938-949.
Masselink, G., Evans, D., Hughes, M.G. and Russell, P., 2005. Suspended sediment transport in the swash zone of a dissipative beach. Marine Geology, 216(3): 169-189.
Masselink, G. and Short, A.D., 1993. The effect of tide range on beach morphodynamics and morphology: A conceptual beach model. Journal of Coastal Research: 785-800.
Mendoza, E. et al., 2014. Beach response to wave energy converter farms acting as coastal defence. Coastal Engineering, 87(0): 97-111.
Millar, D.L., Smith, H.C.M. and Reeve, D.E., 2007. Modelling analysis of the sensitivity of shoreline change to a wave farm. Ocean Engineering, 34(5-6): 884-901.
Ortega-Sánchez, M., Lobo, F.J., López-Ruiz, A., Losada, M.A. and Fernández-Salas, L.M., 2014. The influence of shelf-indenting canyons and infralittoral prograding wedges on coastal morphology: The carchuna system in southern spain. Marine Geology, 347(0): 107-122.
Ortega Sanchez, M., Losada, M. and Baquerizo, A., 2003. On the development of large-scale cuspate features on a semi-reflective beach: Carchuna beach, southern spain. Marine Geology, 198(3): 209-223.
Palha, A., Mendes, L., Fortes, C.J., Brito-Melo, A. and Sarmento, A., 2010. The impact of wave energy farms in the shoreline wave climate: Portuguese pilot zone case study using pelamis energy wave devices. Renewable Energy, 35(1): 62-77.

Poate, T., Masselink, G., Russell, P. and Austin, M., 2014. Morphodynamic variability of high-energy macrotidal beaches, cornwall, uk. Marine Geology, 350(0): 97-111.
Pontes, M. et al., 1996. Weratlas–atlas of wave energy resource in europe. Report to the European Commission, JOULE II Programme, 96p.
Reeve, D.E. et al., 2011. An investigation of the impacts of climate change on wave energy generation: The wave hub, cornwall, uk. Renewable Energy, 36(9): 2404-2413.
Ruol, P., Zanuttigh, B., Martinelli, L., Kofoed, P. and Frigaard, P., 2011. Near-shore floating wave energy converters: Applications for coastal protection, Proceedings of the international conference of Coastal Engineering 2010, Shanghai.
Scott, T., Masselink, G. and Russell, P., 2011. Morphodynamic characteristics and classification of beaches in england and wales. Marine Geology, 286(1–4): 1-20.
Scott, T., Russell, P., Masselink, G., Wooler, A. and Short, A., 2007. Beach rescue statistics and their relation to nearshore morphology and hazards: A case study for southwest england. Journal of Coastal Research, 50: 1-6.
Smith, H.C.M., Pearce, C. and Millar, D.L., 2012. Further analysis of change in nearshore wave climate due to an offshore wave farm: An enhanced case study for the wave hub site. Renewable Energy, 40(1): 51-64.
Stopa, J.E., Cheung, K.F. and Chen, Y.-L., 2011. Assessment of wave energy resources in hawaii. Renewable Energy, 36(2): 554-567.
Tolman, H., 2002. Validation of wavewatch iii version 1.15 for a global domain. Technical Note(213): 33.
US Army Corps Of Engineers, 1984. Shore protection manual. Army Engineer Waterways Experiment Station, Vicksburg, MS. 2v: 37-53.
Veigas, M., Carballo, R. and Iglesias, G., 2014a. Wave and offshore wind energy on an island. Energy for Sustainable Development, 22(0): 57-65.
Veigas, M. and Iglesias, G., 2013. Wave and offshore wind potential for the island of tenerife. Energy Conversion and Management, 76(0): 738-745.
Veigas, M. and Iglesias, G., 2014. Potentials of a hybrid offshore farm for the island of fuerteventura. Energy Conversion and Management, 86(0): 300-308.
Veigas, M., López, M. and Iglesias, G., 2014b. Assessing the optimal location for a shoreline wave energy converter. Applied Energy, 132(0): 404-411.
Veigas, M., Ramos, V. and Iglesias, G., 2014c. A wave farm for an island: Detailed effects on the nearshore wave climate. Energy, 69: 801-812.
Vicinanza, D., Contestabile, P. and Ferrante, V., 2013. Wave energy potential in the north-west of sardinia (italy). Renewable Energy, 50: 506-521.
Vidal, C., Méndez Fernando, J., Díaz, G. and Legaz, R., 2007. Impact of santoña wec installation on the littoral processes. Proceedings of the 7th European wave and tidal energy conference, Porto, Portugal.
Wright, L. and Short, A.D., 1984. Morphodynamic variability of surf zones and beaches: A synthesis. Marine Geology, 56(1): 93-118.
Zanuttigh, B. and Angelelli, E., 2013. Experimental investigation of floating wave energy converters for coastal protection purpose. Coastal Engineering, 80: 148-159.